# Evaluation of longitudinal time-lapsed *in vivo* micro-CT for monitoring fracture healing in mouse femur defect models

Esther Wehrle[1], Duncan C Betts[1], Gisela A Kuhn[1], Ariane C Scheuren[1], Sandra Hofmann[1,2], Ralph Müller[1*]

[1] Institute for Biomechanics, ETH Zurich, Zurich, Switzerland, [2] Department of Biomedical Engineering and Institute for Complex Molecular Systems, Eindhoven University of Technology, The Netherlands.

**Corresponding author:**

Ralph Müller, PhD

Institute for Biomechanics

ETH Zurich

Leopold-Ruzicka-Weg 4

8093 Zurich, Switzerland

Email: ram@ethz.ch

## Abstract

Longitudinal *in vivo* micro-computed tomography (micro-CT) is of interest to non-invasively capture the healing process of individual animals in preclinical fracture healing studies. However, as adverse imaging effects associated with anesthesia, handling, and radiation have been reported in some cases, this study assessed imaging-associated effects on fracture healing in a mouse femur defect model. A scan group received weekly micro-CT measurements (week 0-6), whereas controls were only scanned post-operatively and at week 5 and 6. Registration of consecutive scans enabled assessment of bone turnover with distinct characteristics of the different healing phases. Weekly micro-CT application did not significantly change any of the assessed callus parameters in defect and periosteal volumes. This was supported by histology showing only small amounts of cartilage residuals in both groups, indicating progression towards the end of the healing period. Also, immunohistochemical staining of Sclerostin, previously associated with mediating adverse radiation effects on bone, did not reveal differences between groups.

The established longitudinal *in vivo* micro-CT-based approach allows monitoring of healing phases in mouse femur defect models without significant effects of anesthesia, handling and radiation on callus properties. Therefore, this study supports application of longitudinal *in vivo* micro-CT for healing-phase-specific monitoring of fracture repair in mice.

## Introduction

Adequate monitoring and characterization of the healing process is important in preclinical fracture healing studies. One recent approach to non-invasively capture the formation and remodeling of the osseous fracture callus is the repeated application of *in vivo* micro-computed tomography (micro-CT) [1-3]. This approach allows three-dimensional assessment of callus structures and by registering consecutive scans, dynamic parameters such as bone formation and resorption can be evaluated [4,5]. As each animal can be followed individually throughout the healing process with low variance in the assessed parameters, animal numbers can be reduced compared to well-established cross-sectional studies with endpoint micro-CT and two-dimensional histological callus evaluation.

In non-fractured bone, longitudinal time-lapsed *in vivo* micro-CT has been increasingly used to monitor changes in bone properties associated with different diseases and external factors, e.g. estrogen-deficiency [6-8], mechanical-(un)loading [9-11], and drug application [12]. However, several studies indicate that anesthesia, cumulative radiation dosage and stress due to the required handling for the CT measurements may have effects on animal well-being and bone properties [7,13-16]. According to the EU Directive 2010/63, the severity of repeated isoflurane anesthesia can be categorized as mild, although repeated anesthesia was considered worse than a single session with sex-dependent differences in perceiving the severity of a procedure [13]. Specifically, female mice were shown to be more susceptible to anesthesia-induced effects on well-being compared to male mice. Nevertheless, in both sexes repeated isoflurane anesthesia caused only short-term mild distress and impairment of well-being, mainly in the immediate post-anesthetic period. Radiation has also been shown to have dosage-dependent effects on bone cells *in vivo* and *in vitro* (12): Whereas

high dose x-ray radiation (2.5-8Gy) was associated with reduced osteoblast and osteoclast proliferation [9,17-19], lower doses (<2Gy) had a stimulatory effect on osteoclasts. Some studies reported radiation-associated effects on structural bone parameters, whereas other studies did not see any changes [7,20]. These findings indicate the importance of study-specific adaptation of micro-CT protocols, and to protect animals scanning times and radiation settings should be minimized.

Recently, several fracture healing studies have applied longitudinal *in vivo* micro-CT to monitor callus formation [2,3,21-23]. However, as adverse effects of longitudinal imaging on the development of bone properties have been reported in the literature in some cases during normal bone remodeling, there is a need to also assess imaging-associated impact on the callus formation during the highly metabolically active process of fracture healing.

Therefore, the objectives of this study were to establish an *in vivo* micro-CT based approach for longitudinal monitoring of fracture healing in a mouse femur defect model and to assess the combined effect of radiation, anesthesia and handling associated with weekly time-lapsed micro-CT measurements on callus properties during the remodeling phase of fracture healing.

## Results

### General physical observation

All mice recovered rapidly from surgery. During the healing period, in both groups, the animals' body weight did not significantly change compared to pre-operative values without significant differences between the two groups (see Supplementary Fig. S1 online). Social

86 interaction between mice and nesting behaviour did not differ from pre-surgical
87 observations and was similar for animals of the scan and control groups.
88
89 **Volumes of interest (VOI) for evaluation by time-lapsed *in vivo* micro-CT**
90 One animal from the scan group could not be included in the analysis due to failure in VOI
91 generation caused by too little cortical bone being present in the field of view. The four
92 different VOIs (depicted in Fig. 1) encompassed the following volume for the control (n=8)
93 and scan group (n=10): 2.51±0.34mm$^3$ vs. 2.60±0.34mm$^3$ for the defect center (DC),
94 17.26±2.21mm$^3$ vs. 18.73±4.64mm$^3$ for the defect periphery (DP), 1.86±0.48mm$^3$ vs.
95 1.73±0.45mm$^3$ for the cortical fragments (FC), 14.47±3.30mm$^3$ vs. 13.10±2.66mm$^3$ for the
96 fragment periphery (FP). The total volume (TOT) between the inner pins of the fixator was
97 36.10±2.81mm$^3$ for the control and 36.15±3.74mm$^3$ for the scan group. No significant
98 differences in volume were detected in any of the VOIs between groups.
99
100 **Longitudinal monitoring of fracture healing by time-lapsed *in vivo* micro-CT**
101 In the scan group (n=10), the repeated micro-CT scans (1x/week, Fig. 2) covered the period
102 from the day of the defect surgery (d0) until post-operative week 6 with distinct callus
103 characteristics indicative of the different healing phases (inflammation, repair, remodeling).
104 From week 0-1 to week 1-2 a significant 5.7x increase in bone formation was detected (Fig.
105 3a) in the total VOI (TOT=DC+DF+FC+FP, $p<0.0001$; Fig. 1), indicating progression from the
106 inflammation to the reparative phase. This led to a significant gain in bone volume by week 2
107 ($BV/TV_{week2}$: 39±7% vs. $BV/TV_{week0}$: 25±3%, $p=0.0134$; Fig. 3b). As bone formation triggers the
108 onset of bone resorption, a significant 2.8x increase in resorptive activities was seen from

week 1-2 to week 2-3 (p=0.0020), indicating the progression to the remodeling phase. Two weeks after surgery the highly mineralized bone fraction in the TOT VOI was significantly lower compared to the post-operative measurement ($BV_{645}/BV_{395}$ in week 2: 59±5% vs. $BV_{645}/BV_{395}$ in week 0: 84±1%, $p$<0.0001), indicating formation of mineralized callus of low density. From postoperative week 2 onwards, the highly mineralized bone fraction in the TOT VOI gradually increased in all subsequent weeks of the healing period reaching statistical significance by week 5 ($BV_{645}/BV_{395}$ in week 2: 59±5% vs. $BV_{645}/BV_{395}$ in week 5: 79±3%, p=0.0134; Fig. 3c).

In order to better capture the regions where bone is mainly formed and resorbed, we evaluated the different VOIs separately (Table 1): In the early postoperative phase from week 0-1 to week 1-2 a strong onset of bone formation was seen in the DC and FP sub-volumes, leading to significant 11.8x and 3.4x gain in mineralized tissue from week 0 to week 2 for DC (p=0.0090) and FP (p=0.0091), respectively. This indicates that both intra-cortical as well as periosteal callus formation takes place in this femur defect model. In both VOIs bone formation triggered the initiation of bone resorption from week 2-3. In detail, there was a significant 6.2x and 2.9x increase in bone resorption from week 1-2 to week 2-3 in the DC (p=0.0040) and the FP VOI (p=0.0079), respectively. Compared to the DC and FP VOIs, the initiation of bone formation was much less pronounced in the DP sub-volume with less deposition of mineralized tissue leading to only little peripheral callus formation in this VOI (week 2-6) and subsequently low bone resorption activities from week 2-3 to week 5-6. In all three regions (DC, DP, FP) the fraction of highly mineralized tissue considerably increased from week 2 to week 5 (+192%, +774%, +227%), indicating callus maturation. In this femur

defect model, callus formation and remodeling mainly took place in the defect region (DC) with only little peripheral callus formation and remodeling (DP). Looking at the cortical fragments (FC), a significant 3.2x increase in resorptive activities was detected in week 1-2 compared to week 0-1 ($p=0.0421$), whereas no significant weekly change in bone formation activities was seen in this region throughout the assessed healing period. This resulted in a significant 24% reduction in bone volume from week 0 to week 4 ($p=0.0091$). The fraction of highly mineralized bone also gradually decreased in the remaining osseous tissue reaching statistical significance by week 3 ($BV_{645}/BV_{395}$ in week 3 reduced by 9% compared to week 0, $p=0.0027$).

**Influence of the longitudinal *in vivo* micro-CT protocol on callus properties**

To assess the combined effects of radiation, anesthesia and handling associated with weekly micro-CT measurements (week 0 - week 6) on callus properties, callus parameters of the scan group were compared to control animals that were scanned only directly post-operatively (d0) and after 5 and 6 weeks (Fig. 4).

Post-operatively (d0), no significant group differences in bone volume (BV/TV) were found in any of the VOIs: 1.82±0.39% (control) vs. 1.47±0.15% (scan) in DC, 0.16±0.12% (control) vs. 0.13±0.06% (scan) in DP, 56.82±2.31% (control) vs. 57.14±6.99% (scan) in FC, 4.66±0.30% (control) vs. 4.74±0.76% (scan) in FP. Likewise, no group differences in bone volume were seen in the total volume (TOT; 26.92±4.69% in controls and 24.90±2.88% in the scan group).

During the remodeling phase (post-operative weeks 5-6), no significant difference in bone turnover was seen in the total volume (TOT) between the inner pins of the fixator (BFR: 0.76±0.23% in controls, 0.64±0.15% in scan group; BRR: 0.82±0.25% in controls, 0.78±0.26% in scan group). Also, bone volume did not significantly change due to the applied micro-CT protocol with a similar fraction of highly mineralized tissue after 5 weeks ($BV_{645}/BV_{395:}$ 79±3% in controls, 79±3% in scan group) and 6 weeks ($BV_{645}/BV_{395}$: 81±3% in controls, 82±4% in scan group).

Regarding the four sub-volumes (Table 2), the applied micro-CT protocol did not significantly affect bone formation and resorption activities in the callus VOIs (DC, DP and FP) from week 5-6 with similar bone volume observed in week 5 and 6 for controls and scanned animals. In both groups, bone volume remained stable from week 5 to week 6, whereas the density of the mineralized tissue increased during the same period (DC, DP, FP). Looking at the adjacent cortical fragments (FC) also no significant differences were detected in any of the assessed parameters between the control group and the scan group. Similarly to the callus VOIs, bone volume also remained stable in this region from week 5 to week 6. However, in contrast to the callus VOIs, the density of the mineralized tissue in the cortical VOI FC did not change from week 5 to week 6. In week 6, the FC VOI comprised 33% and 35% of the osseous tissue in the total VOI (TOT) for the control and scan group, respectively. In the DC VOI, 37% (control group) and 36% (scan group) of the total bone volume were seen. Less osseous tissue was detected in the two peripheral VOIs, 11% (control group) and 12% (scan group) in the DP and 19% (control group) and 17% (scan group) in the FP VOI.

As group comparisons were only performed from week 5-6, we particularly focused on the defect VOIs (DC+DP) which are most important for evaluating later healing time points during the remodeling phase of fracture healing. No significant differences in bone turnover, bone volume and mineralization were seen between the scan and control group. In addition, according to the standard clinical evaluation of X-rays, the number of bridged cortices per callus was evaluated in two perpendicular planes and animals with ≥3 bridged cortices were categorized as healed. By week 5, cortical bridging occurred in 75% of the control animals and 64% of the scanned animals (Table 3). However, non-unions only occurred in defects of ≥1.5mm length. Taking into account only these defects (≥1.5mm length), both groups had a non-union rate of 67% indicating no significant effect of the chosen micro-CT protocol on clinical fracture healing outcome.

**Histology**

As shown by Safranin-O staining six weeks after osteotomy no cartilage residuals were present in the defect region in the bridged defects indicating normal progression of the healing process in the final remodeling stage. In the non-union defects, only small areas of cartilage were seen in the defect region. No differences were seen by visual inspection between animals from the scan and control group (Fig. 5).

As radiation-mediated decreased bone formation by osteoblasts has previously been associated with the inhibition of osteoanabolic Wnt-signaling [24], we assessed Sclerostin expression in the defect region by immunohistochemistry. Visual inspection did not reveal

any differences in staining intensity and amount of Sclerostin between the scan and control group (Fig. 5).

## Discussion

In this study, longitudinal *in vivo* micro-CT was applied for monitoring the process of fracture healing in mice. In addition, the combined effect of radiation, anesthesia and handling associated with the established imaging approach on callus parameters was assessed. Until now, preclinical fracture healing studies predominantly have a cross-sectional study design with end-point callus evaluation in sub-groups of animals at different time points during the healing period. Only recently, several studies in murine diaphyseal femur defect models stabilized by external fixation [2,3,21,22] or intramedullary nails [23], have applied longitudinal *in vivo* micro-CT to monitor the healing progression in each animal over time. These studies were able to consecutively assess callus parameters (e.g. callus volume and density) at specific time points during the healing process for up to 12 weeks [2,3,21-23]. By registering consecutive scans, we were now able to include dynamic parameters such as bone formation and resorption in our micro-CT based monitoring approach for fracture healing. This allows for characterization of the different healing phases seen by changes in formation and resorption in the osseous callus volume.

Specifically, we saw that the initiation of bone formation (maximum in week 2-3), indicative of the onset of the reparative phase, triggered bone resorption (maximum in week 3-4) with maximum osseous callus volumes in week 3. From week 4 to week 6, bone formation and resorption continuously decreased. Whereas these remodeling activities also led to a decrease in callus volume from week 4 to week 6, the density of the mineralized tissue in the

222 callus increased during the same period indicating advanced callus maturation. These
223 observations were further supported by histology with no remaining cartilage in the defect
224 region of unions and only a small amount of cartilage residuals in some non-unions. The
225 findings are also in accordance with previous longitudinal studies of up to 4 weeks in mice
226 [2,3,22] and 8 weeks in rats [21] mainly focusing on the inflammation and reparative phase.
227 Similar to our study, the bone volume continuously increased during the 4/8 week healing
228 period, although no remodeling to the original bone geometry was seen due to the shorter
229 observation period. One study in ovariectomized rats with a 12-week post-operative
230 monitoring period detected maximum osseous callus volumes by week 6, which diminished
231 thereafter, whereas bone mineral density continuously increased until week 12, similar to
232 our findings. This indicates that during the reparative phase first low-density bone is formed,
233 which is then further mineralized during the remodeling phase of fracture healing. Looking
234 at the functional fracture healing outcome, complete cortical bridging was seen in 64% of
235 the animals, which is similar to other studies (60-62%) using similar femur defect models
236 with relatively stiff external fixation (fixator stiffness measured in our study 24N/mm) in
237 mice [2,25]. However, differences in defect sizes have to be considered: 0.7mm [2], 1.19±0.25
238 mm [25], 1.47±0.16mm (this study). In contrast to the other studies, we saw the manifestation
239 of non-unions only in defects ≥1.5mm. This might be partially due to the fact that in some
240 studies the exact defect length might have differed from the reported value (saw diameter
241 used for osteotomy) and that non-union formation was assessed irrespective of defect
242 length. Overall, all longitudinal fracture healing studies using *in vivo* micro-CT were able to
243 follow the healing progression in single animals, thereby reducing variance of outcome
244 parameters compared to cross-sectional studies, also allowing for reduction of animals per

group considering the 3R principles of animal welfare [26,27]. However, when applying longitudinal *in vivo* micro-CT, the effect of repeated anesthesia, handling and radiation associated with the scans on the study's main outcome parameters and the general well-being of the animals have to be considered.

In this study, isoflurane was used as anesthetic agent for the *in vivo* micro-CT scans, which is the most commonly used inhalation anesthetic in longitudinal imaging studies with a fast on- and offset of anesthesia and low metabolism rate [13]. Despite its general use, isoflurane has been associated with several adverse effects, such as hepatic degenerative changes [28], immunomodulation [29], oxidative DNA damage [30] as well as alterations in expression profiles of oncogene and tumor suppressor genes in the bone marrow [31], which might potentially also affect fracture healing and the general well-being of the animals. A recent study by Hohlbaum et al. (2017) [13], which assessed the impact of repeated isoflurane anesthesia (6 times for 45 min at an interval of 3–4 days) and the associated handling on the well-being of adult C57BL/6JRj mice, categorized the degree of distress as mild according to the EU Directive 2010/63 with only short-term impairment of well-being, mainly in the immediate post-anesthetic period. Therefore, isoflurane-based inhalation anesthesia and the associated handling of the animal is suggested for longitudinal studies with multiple anesthetic sessions per animal.

In this study, the applied micro-CT settings (55 kVp, 145 µA, 350 ms integration time, 500 projections per 180°, 21 mm field of view (FOV), scan duration ca. 15 min) were adapted from well-established protocols used for longitudinal monitoring of bone adaptation and implant integration in tail vertebrae in mice [10,32]. These settings are similar to protocols used in 2 of the 5 longitudinal fracture healing studies published so far [3,21], while the 3 other

studies did not specify the CT settings [2,22,23]. The radiation dosage (CT dose index, CTDI) associated with each scan in the current study was previously estimated to be 0.67 Gy per scan [32,33]. A radiation control experiment using similar settings did not show detrimental effects of 5 weekly *in vivo* micro-CT scans on bone development in tail vertebrae of mice [33].

However, some studies in non-fractured bone indicate cumulative radiation-associated effects on bone properties particularly when using high radiation doses (>2G; [15]). The radiation effects also depend on animal age [15,34] and ovariectomy (OVX) [7], with younger and ovariectomized animals being more susceptible to radiation. So far, only one study assessed radiation-associated effects of longitudinal *in vivo* micro-CT on bone healing in a uni-cortical tibia burr-hole defect model, and did not find significant radiation effects on bone properties [1]. In this study, similar CT settings (45kVp, 133 µA, 200 ms integration time, 1000 projections per 180°) were used; however, due to the smaller dimensions of the defect and resulting shorter scanning time, the radiation dosage (0.36 Gy) was lower compared to our protocol (0.64 Gy).

In the current study, we assessed the combined imaging-associated impact (anesthesia, handling, radiation; 1x/week for 6 weeks) on callus formation and remodeling in a diaphyseal femur defect model in adult female C57BL/6J mice. We did not see any significant imaging-associated changes in bone volume and turnover in the fracture callus during the remodeling phase (post-operative week 5 and 6). Furthermore, no significant differences in callus mineralization between scanned (d0, week1-6) and control animals (d0, week 5+6) in any of the assessed callus volumes (TOT, DC, DP, FP) were observed. The distribution of the osseous callus volume into the three sub-volumes was also not significantly different between groups, indicating similar healing patterns. In addition, when separately assessing

the cortical fragments between the inner pins (FC), also no significant differences in any of the assessed parameters were detected between groups. In respect to clinical healing outcome, the percentage of unions in animals above the sub-critical defect length was 67% in both groups. Defects without cortical bridging only showed small cartilage residuals as visualized by Safranin-O staining, indicating manifestation of non-union formation. In the defect regions of unions, no cartilage was seen, indicating progression towards the end of the healing period. As adverse effects of radiation on bone properties have been shown to be mediated via Sclerostin inhibition of osteoanabolic Wnt-signaling [24], we also visualized Sclerostin expression in the fracture callus by immunohistochemistry, but did not see differences in number of stained osteocytes, staining intensity and pattern between groups in any of the assessed callus regions.

In summary, we did not see significant differences in a total of 7 assessed CT and histological parameters in the total volume (TOT) between the inner pins of the fixator as well as in the different callus sub-volumes (DC, DP, FP) and the adjacent cortical fragments (FC) between the scan and the control group. The sub-volume specific analysis also allowed capturing of distinct features only present in one region (e.g. significant post-operative increase in bone resorption in FC), that showed contrary progression compared to the overall picture (significant post-operative increase in bone formation in DC, DP and FP). This also shows the importance of VOI selection. The other longitudinal fracture healing studies either assessed a VOI consisting of the defect as well as adjacent bone fragments, or then only the callus in the defect region including the last slice of intact cortex [2,3], or the callus in the defect and periosteal region combined [21] was evaluated. An overall VOI including the defect region and cortical fragments can give an overview of callus characteristics, but sub-volume-specific

differences might be missed. Therefore, analysis of different endosteal and periosteal callus regions as well as the adjacent cortical volume is favorable.

The longitudinal *in vivo* micro-CT based approach established in this study allows monitoring of the different healing phases in mouse femur defect models without significant anesthesia-, handling- and radiation-associated effects on callus properties. By registering consecutive scans of the defect region for each animal, data on bone turnover can be obtained with distinct characteristics of the different fracture healing phases. Importantly, repeated anesthesia, handling and radiation associated with the scans did not impair callus formation and remodeling. Therefore, this study supports the application of longitudinal *in vivo* micro-CT for healing-phase specific monitoring of fracture repair in mice. Further studies should evaluate the potential of this micro-CT-based monitoring approach for healing phase-specific discrimination of normal and impaired healing conditions.

## Methods

### Study design

A micro-CT based approach for longitudinal *in vivo* monitoring of fracture healing was established for a mouse femur defect model. All mice received a femur defect and post-operative micro-CT scans (vivaCT 40, ScancoMedical, Brüttisellen, Switzerland) were performed. The scan group then received weekly scans of the defect area (weeks 1-6). To assess the combined effect of radiation, anesthesia and handling associated with weekly micro-CT measurements, controls were only scanned after 5 weeks. Control animals then received another scan in post-operative week 6 to enable the assessment of both, static and dynamic bone parameters during the final remodeling phase of fracture healing.

337

338 **Animals**

339 All animal procedures were approved by the authorities (licence number: 36/2014;
340 Kantonales Veterinäramt Zürich, Zurich, Switzerland). We confirm that all methods were
341 carried out in accordance with relevant guidelines and regulations (ARRIVE guidelines and
342 Swiss Animal Welfare Act and Ordinance (TSchG, TSchV)). Female 12 week-old C57BL/6J
343 mice were purchased from Janvier (Saint Berthevin Cedex, France) and housed in the animal
344 facility of the ETH Phenomics Center (EPIC; 12h:12h light-dark cycle, maintenance feed
345 (3437, KLIBA NAFAG, Kaiseraugst, Switzerland), 5 animals/cage). At an age of 20 weeks, all
346 animals received a femur defect by performing an osteotomy (group 1: control group, defect
347 length - 1.45mm ± 0.16, n=8; group 2: scan group, defect length -1.47mm ± 0.16, n=11;
348 housing after surgery: 2-3 animals/cage). Perioperative analgesia (25 mg/L, Tramal®,
349 Gruenenthal GmbH, Aachen, Germany) was provided via the drinking water two days before
350 surgery until the third postoperative day. For surgery and micro-CT scans, animals were
351 anesthetized with isoflurane (induction/maintenance: 5%/1-2% isoflurane/oxygen).

352

353 **Femur osteotomy**

354 An external fixator (Mouse ExFix, RISystem, Davos, Switzerland; stiffness: 24N/mm [35]) was
355 positioned at the craniolateral aspect of the right femur and attached using four mounting
356 pins. First, the most distal pin was inserted approximately 2mm proximal to the growth
357 plate, followed by placement of the most proximal and the inner pins. Subsequently, a femur
358 defect was created using 2 Gigli wire saws.

359

360 **Time-lapsed *in vivo* micro-CT**

361 Immediate post-surgery correct positioning of the fixator and the defect was visualized using
362 a vivaCT 40 (Scanco Medical AG, Brüttisellen, Switzerland) (isotropic nominal resolution: 10.5
363 µm; 2 stacks of 211 slices; 55 kVp, 145 µA, 350 ms integration time, 500 projections per
364 180°, 21 mm field of view (FOV), scan duration ca. 15 min). Subsequently, the fracture callus
365 and the adjacent bone between the inner pins of the fixator were scanned weekly using the
366 same settings. Scans were registered consecutively and morphometric indices (bone volume
367 - BV, bone volume/total volume – BV/TV, bone formation rate – BFR, bone resorption rate -
368 BRR) were computed (threshold: 395mg HA/$cm^3$; [4,11]). To assess mineralization progression,
369 a second threshold (645mg HA/$cm^3$) was applied and the ratio between highly and lowly
370 mineralized tissue ($BV_{645}/BV_{395}$) was calculated. According to the standard clinical evaluation
371 of X-rays, the number of bridged cortices per callus was evaluated in two perpendicular
372 planes (UCT Evaluation V6.5-1, Scanco Medical AG, Brüttisellen, Switzerland). A ‘‘healed
373 fracture’’ was considered as having a minimum of at least three bridged cortices per callus.
374 For evaluation, four volumes of interest (VOIs) were defined, which were created
375 automatically from the post-operative measurement (Fig. 1): defect center (DC), defect
376 periphery (DP), cortical fragment center (FC), and fragment periphery (FP). Data were
377 normalised to the central VOIs: DC/DC, DP/DC, FC/FC, FP/FC.
378
379 **Histology**
380 Histological analyses were performed in a sub-set of animals (n=6/group). On day 42, femora
381 were excised, the femoral head was removed and the samples were placed in 4% neutrally
382 buffered formalin for 24 hours and subsequently decalcified in 12.5% EDTA for 10-14 days.

The samples were embedded in paraffin and 4.5 µm longitudinal sections were stained with Safranin-O/Fast Green: Weigert's iron haematoxylin solution (HT1079, Sigma-Aldrich, St. Louis, MO) - 4min, 1:10 HCl-acidified 70% ethanol - 10s, tap water - 5min, 0.02% Fast Green (F7258, Sigma-Aldrich, St. Louis, MO) - 3min, 1% acetic acid - 10s, 0.1% Safranin-O (84120, Fluka, St. Louis, MO) - 5min. Images were taken with Slide Scanner Pannoramic 250 (3D Histech, Budapest, Hungary) at 20x magnification.

For immunohistochemical staining of Sclerostin, nonspecific sites were blocked (1% BSA/PBS + 1% rabbit serum) for 60 min at room temperature. Subsequently, the sections were incubated with the primary antibody against Sclerostin (AF1589, R&D Systems, Minneapolis, MN; 1:150 in 1%BSA/PBS + 0.2% rabbit serum) overnight at 4°C. To detect the primary antibody, a secondary biotinylated rabbit anti-goat-IgG antibody (BAF017, R&D Systems, Minneapolis, MN) was added for 1 h at room temperature. For signal amplification, the slides were incubated with avidin-biotin complex (PK-6100 Vector Laboratories, Burlingame, CA) for 30 min. Diaminobenzidine (Metal Enhanced DAB Substrate Kit, 34065 ThermoFisher Scientific, Waltham, MA) was used as detection substrate. Counterstaining was performed with FastGreen (F7258, Sigma-Aldrich, St. Louis, MO). Species-specific IgG was used as isotype control. Images were taken with Slide Scanner Pannoramic 250 (3D Histech, Budapest, Hungary) at 40x magnification.

**Statistics**

CT analysis: Data were tested for normal distribution (Shapiro-Wilk-Test) and homogeneity of variance (Levene-Test). Depending on the test outcome, group comparisons (scan versus

control group) of data derived at single time points were performed by two-tailed Student's t-test or Mann-Whitney U-test (IBM SPSS Statistics Version 23). For statistical evaluation of repeated measurements (scan group) dependent on results from normality and variance tests, either one-way analysis of variance (ANOVA) with Bonferroni correction or Friedman test with Dunn correction for multiple comparisons (GraphPad Prism 7) were performed. Two-way ANOVA was used for longitudinal comparison of the body weight between the control and the scan group. The level of significance was set at $p < 0.05$.

**Acknowledgements**

The authors gratefully acknowledge support from the EU (BIODESIGN FP7-NMP-2012-262948 and ERC Advanced MechAGE ERC-2016-ADG-741883). E. Wehrle received funding from the ETH Postdoctoral Fellowship Program (MSCA-COFUND, FEL-25_15-1).

**Author Contributions Statement**

The study was designed by E.W., G.A.K., S.H. and R.M.. The experiments were performed by E.W., G.A.K. and A.C.S.. Data analyses were performed by E.W. and D.C.B.. The manuscript was written by E.W. and reviewed and approved by all authors.

**Data availability**

All necessary data generated or analyzed during the present study are included in this published article and its Supplementary Information files (preprint available on BioRxiv (BIORXIV/2019/692343). Additional information related to this paper may be requested from the authors.

## Competing Interests

The authors declare no competing interests.

## References


1 Taiani, J. T. *et al.* Embryonic stem cell therapy improves bone quality in a model of impaired fracture healing in the mouse; tracked temporally using in vivo micro-CT. *Bone* **64**, 263-272, doi:10.1016/j.bone.2014.04.019 (2014).

2 Locher, R. J. *et al.* Traumatic brain injury and bone healing: radiographic and biomechanical analyses of bone formation and stability in a combined murine trauma model. *J. Musculoskel. Neuron.* **15**, 309-315 (2015).

3 Graef, F. *et al.* Impaired fracture healing with high non-union rates remains irreversible after traumatic brain injury in leptin-deficient mice. *J. Musculoskel. Neuron.* **17**, 78-85 (2017).

4 Betts, D., Wehrle, E., Kuhn, G. A., Hofmann, S. & Müller, R. Quantification of mechanical stimuli and bone formation in fracture healing using in vivo time-lapsed imaging. *Tissue Eng. Pt. A* **21**, S56-S56 (2015).

5 Wehrle, E., Kuhn, G. A., Betts, D. C., Scheuren, A. & Müller, R. Influence of longitudinal in vivo micro-computed tomography on fracture healing in a femoral defect model. *Tissue Eng. Pt. A* **21**, S406-S406 (2015).

6 Boyd, S. K., Davison, P., Müller, R. & Gasser, J. A. Monitoring individual morphological changes over time in ovariectomized rats by in vivo micro-computed tomography. *Bone* **39**, 854-862, doi:10.1016/j.bone.2006.04.017 (2006).

7 Klinck, R. J., Campbell, G. M. & Boyd, S. K. Radiation effects on bone architecture in mice and rats resulting from in vivo micro-computed tomography scanning. *Med. Eng. Phys.* **30**, 888-895, doi:10.1016/j.medengphy.2007.11.004 (2008).

8 Lambers, F. M., Kuhn, G., Schulte, F. A., Koch, K. & Müller, R. Longitudinal assessment of in vivo bone dynamics in a mouse tail model of postmenopausal osteoporosis. *Calcified Tissue Int.* **90**, 108-119, doi:10.1007/s00223-011-9553-6 (2012).

9 David, V. *et al.* Noninvasive in vivo monitoring of bone architecture alterations in hindlimb-unloaded female rats using novel three-dimensional microcomputed tomography. *J. Bone Miner. Res.* **18**, 1622-1631, doi:10.1359/jbmr.2003.18.9.1622 (2003).

10 Lambers, F. M., Schulte, F. A., Kuhn, G., Webster, D. J. & Müller, R. Mouse tail vertebrae adapt to cyclic mechanical loading by increasing bone formation rate and decreasing bone resorption rate as shown by time-lapsed in vivo imaging of dynamic bone morphometry. *Bone* **49**, 1340-1350, doi:10.1016/j.bone.2011.08.035 (2011).

11 Schulte, F. A., Lambers, F. M., Kuhn, G. & Müller, R. In vivo micro-computed tomography allows direct three-dimensional quantification of both bone formation and bone resorption parameters using time-lapsed imaging. *Bone* **48**, 433-442, doi:10.1016/j.bone.2010.10.007 (2011).

12 Kuhn, G., Weigt, C., Lambers, F. M., Schulte, F. A. & Müller, R. Bisphosphonate treatment does not impair load adaptation in osteopenic mouse bones. *Bone* **50**, S156-S156, doi:10.1016/j.bone.2012.02.487 (2012).

13 Hohlbaum, K. *et al.* Severity classification of repeated isoflurane anesthesia in C57BL/6JRj mice-Assessing the degree of distress. *Plos One* **12**, doi:ARTN e017958810.1371/journal.pone.0179588 (2017).

14 Tremoleda, J. L. *et al.* Imaging technologies for preclinical models of bone and joint disorders. *Ejnmmi Res.* **1**, doi:Artn 1110.1186/2191-219x-1-11 (2011).

15 Laperre, K. *et al.* Development of micro-CT protocols for in vivo follow-up of mouse bone architecture without major radiation side effects. *Bone* **49**, 613-622, doi:10.1016/j.bone.2011.06.031 (2011).

16 Hildebrandt, I. J., Su, H. & Weber, W. A. Anesthesia and other considerations for in vivo imaging of small animals. *ILAR J.* **49**, 17-26 (2008).

17 Dudziak, M. E. *et al.* The effects of ionizing radiation on osteoblast-like cells in vitro. *Plast. Reconstr. Surg.* **106**, 1049-1061 (2000).

18 Matsumura, S., Jikko, A., Hiranuma, H., Deguchi, A. & Fuchihata, H. Effect of X-ray irradiation on proliferation and differentiation of osteoblast. *Calcified Tissue Int.* **59**, 307-308 (1996).

19 Scheven, B. A. A., Burger, E. H., Kawilarangdehaas, E. W. M., Wassenaar, A. M. & Nijweide, P. J. Effects of ionizing irradiation on formation and resorbing activity of osteoclasts in vitro. *Lab. Invest.* **53**, 72-79 (1985).

20 Brouwers, J. E. M., Van Rietbergen, B. & Huiskes, R. No effects of in vivo micro-CT radiation on structural parameters and bone marrow cells in proximal tibia of Wistar rats detected after eight weekly scans. *J. Orthop. Res.* **25**, 1325-1332, doi:10.1002/jor.20439 (2007).

21 Mehta, M., Checa, S., Lienau, J., Hutmacher, D. & Duda, G. N. In vivo tracking of segmental bone defect healing reveals that callus patterning is related to early mechanical stimuli. *Eur. Cells Mater.* **24**, 358-371; discussion 371 (2012).

22 Tsitsilonis, S. *et al.* The effect of traumatic brain injury on bone healing: an experimental study in a novel in vivo animal model. *Injury* **46**, 661-665, doi:10.1016/j.injury.2015.01.044 (2015).

23 Wang, A. Y. *et al.* Effect of cervus and cucumis peptides on osteoblast activity and fracture healing in osteoporotic bone. *Evid. Based Compl. Alt.* **2014**, 958908, doi:10.1155/2014/958908 (2014).

24 Chandra, A. *et al.* Suppression of sclerostin alleviates radiation-induced bone loss by protecting bone-forming cells and their progenitors through distinct mechanisms. *J. Bone Miner. Res.* **32**, 360-372, doi:10.1002/jbmr.2996 (2017).

25 Zwingenberger, S. *et al.* Establishment of a femoral critical-size bone defect model in immunodeficient mice. *J. Surg. Res.* **181**, e7-e14, doi:10.1016/j.jss.2012.06.039 (2013).

26 Russel, W. M. S. & Burch, R. L. *The Principles of Humane Experimental Technique* (1959).

27 Tannenbaum, J. & Bennett, B. T. Russell and Burch's 3Rs Then and Now: The Need for Clarity in Definition and Purpose. *J. Am. Assoc. Lab. Anim.* **54**, 120-132 (2015).

28 Stevens, W. C. *et al.* Comparative toxicities of halothane, isoflurane, and diethyl-ether at subanesthetic concentrations in laboratory-animals. *Anesthesiology* **42**, 408-419, doi:Doi 10.1097/00000542-197504000-00008 (1975).

29 Stollings, L. M. *et al.* Immune modulation by volatile anesthetics. *Anesthesiology* **125**, 399-411, doi:10.1097/Aln.0000000000001195 (2016).

30 Kim, H. *et al.* Oxidative damages in the DNA, lipids, and proteins of rats exposed to isofluranes and alcohols. *Toxicology* **220**, 169-178, doi:10.1016/j.tox.2005.12.010 (2006).

31 Kadar, B. *et al.* Effects of isoflurane exposure on oncogene and tumour suppressor gene expressions in vital organs of CBA/CA mice. *In Vivo* **21**, 861-865 (2007).

32 Li, Z. H., Kuhn, G., Schirmer, M., Müller, R. & Ruffoni, D. Impaired bone formation in ovariectomized mice reduces implant integration as indicated by longitudinal in vivo micro-computed tomography. *Plos One* **12**, doi:ARTN e018483510.1371/journal.pone.0184835 (2017).

33 Lambers, F. M. *et al.* Bone adaptation to cyclic loading in murine caudal vertebrae is maintained with age and directly correlated to the local micromechanical environment. *J. Biomech.* **48**, 1179-1187, doi:10.1016/j.jbiomech.2014.11.020 (2015).

34 Willie, B. M. *et al.* Diminished response to in vivo mechanical loading in trabecular and not cortical bone in adulthood of female C57Bl/6 mice coincides with a reduction in deformation to load. *Bone* **55**, 335-346, doi:10.1016/j.bone.2013.04.023 (2013).

35 Paul, G. R., Cherbuin, M., Wehrle, E. & Müller, R. Minimising external fixator stiffness variation via computational analysis. *Annual Meeting, Swiss Soc. Biomed. Eng*, 45 (2017).

## Figure Legends

**Figure 1.** Volumes of interest (VOIs) for micro-CT evaluation of callus and adjacent bone: Defect center (DC - red), defect periphery (DP - yellow), fragment center (FC - blue), fragment periphery (FP - orange).

**Figure 2.** Representative images (full image and cut; threshold: 645 mg HA/cm$^3$) of the defect region from animals of the scan group (week 0-6): union defect (top panel), non-union defect (bottom panel). Visualization of bone formation (orange) and resorption (blue) via registration of micro-CT scans from week 5 and 6.

**Figure 3**. Micro-CT based evaluation of bone parameters in the scan group using different VOIS: total VOI (TOT) - defect and adjacent bone fragments (top), defect VOI (DC+DP) – defect center and periphery (bottom). a+d. Bone formation rate (solid) and bone resorption rate (dashed line) in the femur defect (TV) given in percent per day. b+e: Bone volume (BV) normalized to TV (DC+FC for TOT and DC for DC+DP). c+f: Degree of bone mineralization given as ratio of bone volume with a density ≥645 mg HA/cm$^3$ to the total osseous volume in the defect (threshold ≥395 mg HA/cm$^3$). n=10; * indicates $p < 0.05$ between consecutive weeks determined by Friedman test with Dunn correction for multiple comparisons (a-e)/ repeated measurements ANOVA with Bonferroni correction (f).

549 **Figure 4.** Micro-CT based evaluation of bone parameters in the scan (red) and control group
550 (blue) using different VOIS: total VOI (TOT) - defect and adjacent bone fragments (top),
551 defect VOI (DC+DP) – defect center and periphery (bottom). a+d. Formed (solid) and
552 resorbed (empty) bone volume (BV) in the femur defect (TV) given in percent per day. b+e:
553 Bone volume (BV) normalized to TV (DC+FC for TOT and DC for DC+DP). c+f: Degree of bone
554 mineralization given as ratio of bone volume with a density ≥645 mg HA/cm$^3$ to the total
555 osseous volume in the defect (threshold ≥395 mg HA/cm$^3$). Control group: n=8, scan group:
556 n=10. * indicates $p < 0.05$ determined by two-tailed Student's t-test (a-e; f: week 6)/Mann-
557 Whitney U-test (f: week 5).

558

559 **Figure 5.** Representative longitudinal sections of fractured femora 6 weeks after defect
560 surgery of unions and non-unions in the scan and control group. Top panel: Safranin-O
561 staining - overview images, scale bar = 2 mm; mid panel: Safranin-O staining – area between
562 inner pins of fixator, scale bar = 500 µm; bottom panel: Sclerostin staining – area centered
563 between inner pins of fixator, scale bar = 100 µm.

564

565 **Tables**

566 **Table 1.** Micro-CT based evaluation of bone parameters in the scan group using different VOIS

| | | Post-operative week | | | | | | | | Post-operative week | | | | | | | |
|---|---|---|---|---|---|---|---|---|---|---|---|---|---|---|---|---|---|
| | | 0-1 | 1-2 | 2-3 | 3-4 | 4-5 | 5-6 | p-value # | | 0 | 1 | 2 | 3 | 4 | 5 | 6 | p-value # |
| **DC** | BFR [%/day] | 0.23 ± 0.10* | 2.24 ± 1.20 | 2.40 ± 1.15 | 1.30 ± 0.49 | 0.63 ±0.14 | 0.41 ± 0.09 | < 0.0001 | BV/TV [%] | 1 ± 0 | 3 ± 1 | 17 ± 9* | 28 ± 15 | 30 ± 14 | 29 ± 12 | 28 ± 10 | < 0.0001 |
| | BRR [%/day] | 0.06 ± 0.02 | 0.14 ± 0.04* | 0.88 ± 0.36 | 1.06 ± 0.85 | 0.75 ± 0.43 | 0.52 ± 0.25 | < 0.0001 | $BV_{645}/BV_{395}$ [%] | 1 ± 1 | 34 ± 10 | 26 ± 6 | 49 ± 7 | 67 ± 6 | 76 ± 6 | 80 ± 6 | < 0.0001 |
| **DP** | BFR [%/day] | 0.03 ± 0.02* | 0.38 ± 0.16 | 1.07 ± 0.88 | 0.68 ± 0.52 | 0.28 ± 0.20 | 0.18 ± 0.11 | < 0.0001 | BV/TV [%] | 0 ± 0 | 0 ± 0 | 3 ± 1 | 9 ± 7 | 11 ± 9 | 11 ± 9 | 11 ± 8 | < 0.0001 |
| | BRR [%/day] | 0.01 ± 0.0 | 0.03 ± 0.02 | 0.19 ± 0.08 | 0.34 ± 0.31 | 0.30 ± 0.23 | 0.18 ± 0.16 | < 0.0001 | $BV_{645}/BV_{395}$ [%] | 2 ± 3 | 24 ± 11 | 8 ± 2 | 37 ± 9 | 61 ± 10 | 71 ± 7 | 74 ± 9 | < 0.0001 |
| **FC** | BFR [%/day] | 0.22 ± 0.08 | 0.26 ± 0.15 | 0.31 ± 0.12 | 0.44 ± 0.19 | 0.45 ± 0.11 | 0.40 ± 0.12 | 0.0019 | BV/TV [%] | 57 ± 7 | 57 ± 6 | 53 + 6 | 48 ± 5 | 44 ± 5 | 41 ± 6 | 40 ± 7 | < 0.0001 |
| | BRR [%/day] | 0.24 ± 0.17* | 0.78 ± 0.31 | 1.13 ± 0.30 | 1.01 ± 0.30 | 0.80 ± 0.25 | 0.60 ± 0.21 | < 0.0001 | $BV_{645}/BV_{395}$ [%] | 95 ± 1 | 92 ± 1 | 89 ±2 | 87 ± 1 | 86 ± 2 | 86 ± 2 | 86 ± 3 | < 0.0001 |
| **FP** | BFR [%/day] | 0.43 ± 0.09* | 1.81 ± 0.58 | 1.77 ± 0.76 | 0.85 ± 0.41 | 0.51 ± 0.28 | 0.33 ± 0.20 | < 0.0001 | BV/TV [%] | 5 ± 1 | 6 ± 1 | 16 ± 4 | 21 ± 7 | 20 ± 8 | 20 ± 9 | 20 ± 9 | < 0.0001 |
| | BRR [%/day] | 0.20 ± 0.09 | 0.40 ± 0.13* | 1.16 ± 0.30 | 0.90 ± 0.38 | 0.57 ± 0.22 | 0.35 ± 0.14 | < 0.0001 | $BV_{645}/BV_{395}$ [%] | 0 ± 0 | 34 ± 9 | 23 ± 7 | 52 ± 7 | 69 ± 5 | 75 ± 4 | 78 ± 3 | < 0.0001 |

567 DC = defect center, DP = defect periphery, FC = cortical fragment center, FP = cortical fragment periphery; BFR – bone formation rate; BRR – bone resorption rate; BV/TV - bone
568 volume normalized to DC for DC, DP and FC for FC, FP; BV645/BV395 - degree of bone mineralization given as ratio of bone volume with a density ≥645 mg HA/$cm^3$ to the total
569 osseous volume (threshold: 395mg HA/$cm^3$); *, significant difference compared to subsequent week ($p < 0.05$); #, p-value over time as tested with repeated measurements
570 ANOVA with Bonferroni correction/Friedman test with Dunn correction for multiple comparisons, n=10

571 **Table 2.** CT evaluation of bone parameters in the different volumes of interest (VOI) for the
572 scan and control group

| VOI | Parameter | Evaluation time point/period | Control group | Scan group |
|---|---|---|---|---|
| DC | BFR [%/day] | week 5-6 | 0.59 ± 0.24 | 0.41 ± 0.09 |
| | BRR [%/day] | week 5-6 | 0.62 ± 0.28 | 0.52 ± 0.25 |
| | BV/TV [%] | week 5 | 35 ± 11 | 29 ± 12 |
| | | week 6 | 35 ± 11 | 28 ± 10 |
| | $BV_{645}/BV_{395}$ [%] | week 5 | 76 ± 2 | 76 ± 6 |
| | | week 6 | 80 ± 3 | 80 ± 6 |
| DP | BFR [%/day] | week 5-6 | 0.18 ± 0.12 | 0.18 ± 0.11 |
| | BRR [%/day] | week 5-6 | 0.15 ± 0.11 | 0.18 ± 0.16 |
| | BV/TV [%] | week 5 | 11 ± 8 | 11 ± 9 |
| | | week 6 | 11 ± 8 | 11 ± 8 |
| | $BV_{645}/BV_{395}$ [%] | week 5 | 71 ± 7 | 71 ± 7 |
| | | week 6 | 75 ± 6 | 74 ± 9 |
| FC | BFR [%/day] | week 5-6 | 0.44 ± 0.19 | 0.40 ± 0.12 |
| | BRR [%/day] | week 5-6 | 0.63 ± 0.19 | 0.60 ± 0.21 |
| | BV/TV [%] | week 5 | 42 ± 6 | 41 ± 6 |
| | | week 6 | 41 ± 6 | 40 ± 7 |
| | $BV_{645}/BV_{395}$ [%] | week 5 | 84 ± 3 | 86 ± 2 |
| | | week 6 | 84 ± 3 | 86 ± 3 |
| FP | BFR [%/day] | week 5-6 | 0.32 ± 0.09 | 0.33 ± 0.20 |
| | BRR [%/day] | week 5-6 | 0.30 ± 0.09 | 0.35 ± 0.14 |
| | BV/TV [%] | week 5 | 21 ± 8 | 20 ± 9 |
| | | week 6 | 21 ± 8 | 20 ± 9 |
| | $BV_{645}/BV_{395}$ [%] | week 5 | 76 ± 5 | 75 + 4 |
| | | week 6 | 79 ± 4 | 78 + 3 |

573 DC - defect center; DP - defect periphery; FC – fragment center; FP – fragment periphery; BFR – bone
574 formation rate; BRR – bone resorption rate; BV/TV - bone volume normalized to DC for DC, DP and FC
575 for FC, FP. $BV_{645}/BV_{395}$ - degree of bone mineralization given as ratio of bone volume with a density
576 ≥645 mg HA/$cm^3$ to the total osseous volume (threshold: 395mg HA/$cm^3$). Control/scan group -
577 n=8/10; *, significant difference compared to control group, $p < 0.05$, assessed by two-tailed
578 Student's t-test or Mann-Whitney U-test.

579 **Table 3.** Number of bridged cortices per callus evaluated in two perpendicular planes and
580 number of mice with successful fracture healing (≥ 3 bridged cortices) evaluated 5 and 6
581 weeks after the defect surgery.

| | Number of bridged cortices | | | | | Fracture healing outcome | |
|---|---|---|---|---|---|---|---|
| Group | 0 | 1 | 2 | 3 | 4 | Not healed | Healed |
| Scan | | | | | | | |
| all animals | 3 | 0 | 1 | 0 | 7 | 4 | 7 |
| defects ≥ 1.5mm | 3 | 0 | 1 | 0 | 2 | 4 | 2 |
| Control | | | | | | | |
| all animals | 2 | 0 | 0 | 0 | 6 | 2 | 6 |
| defects ≥ 1.5mm | 2 | 0 | 0 | 0 | 1 | 2 | 1 |

582

# Figure 1

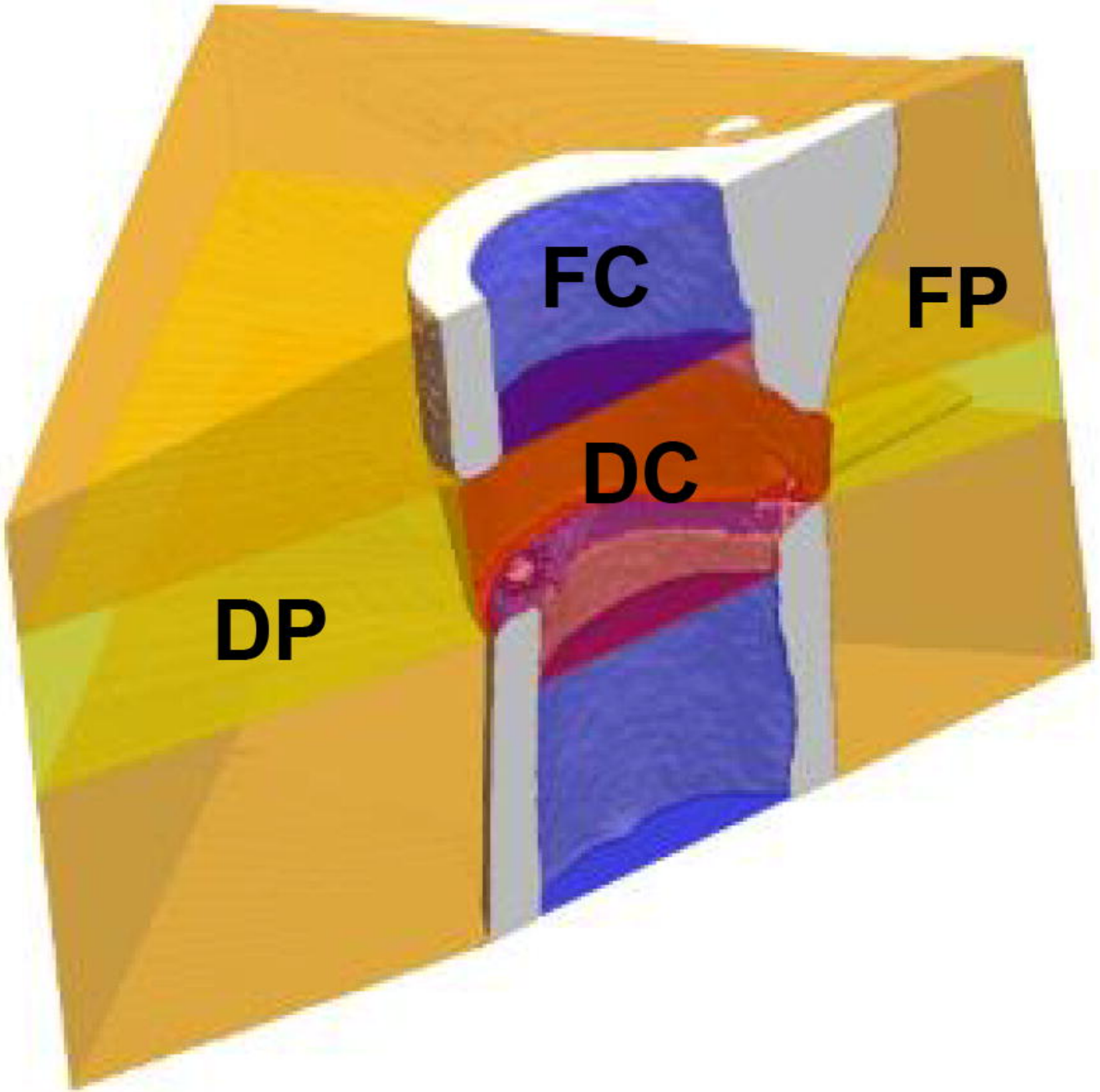

Figure 2

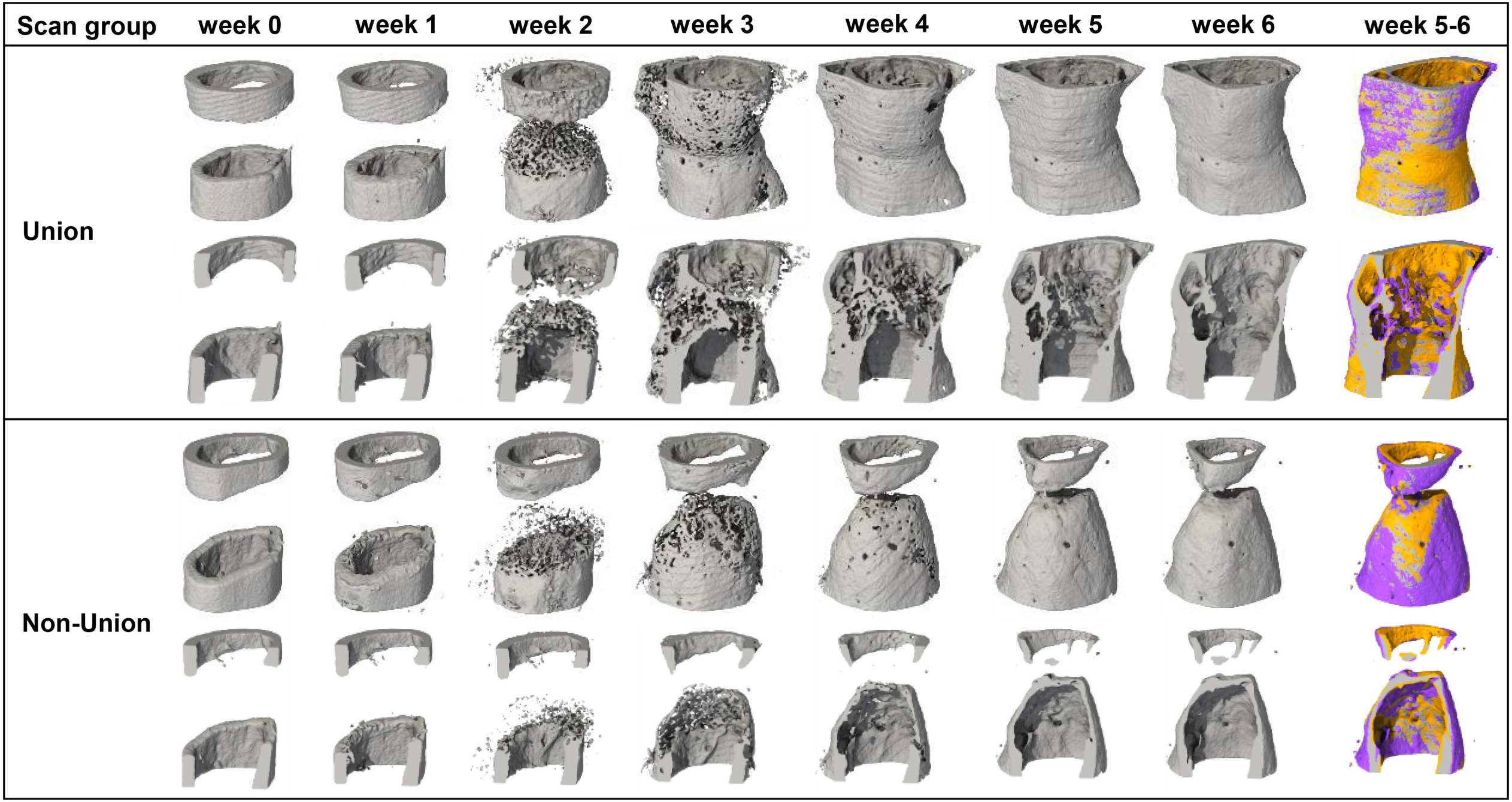
Scan group
week 0
week 1
week 2
week 3
week 4
week 5
week 6
week 5-6
Union
Non-Union

Figure 3

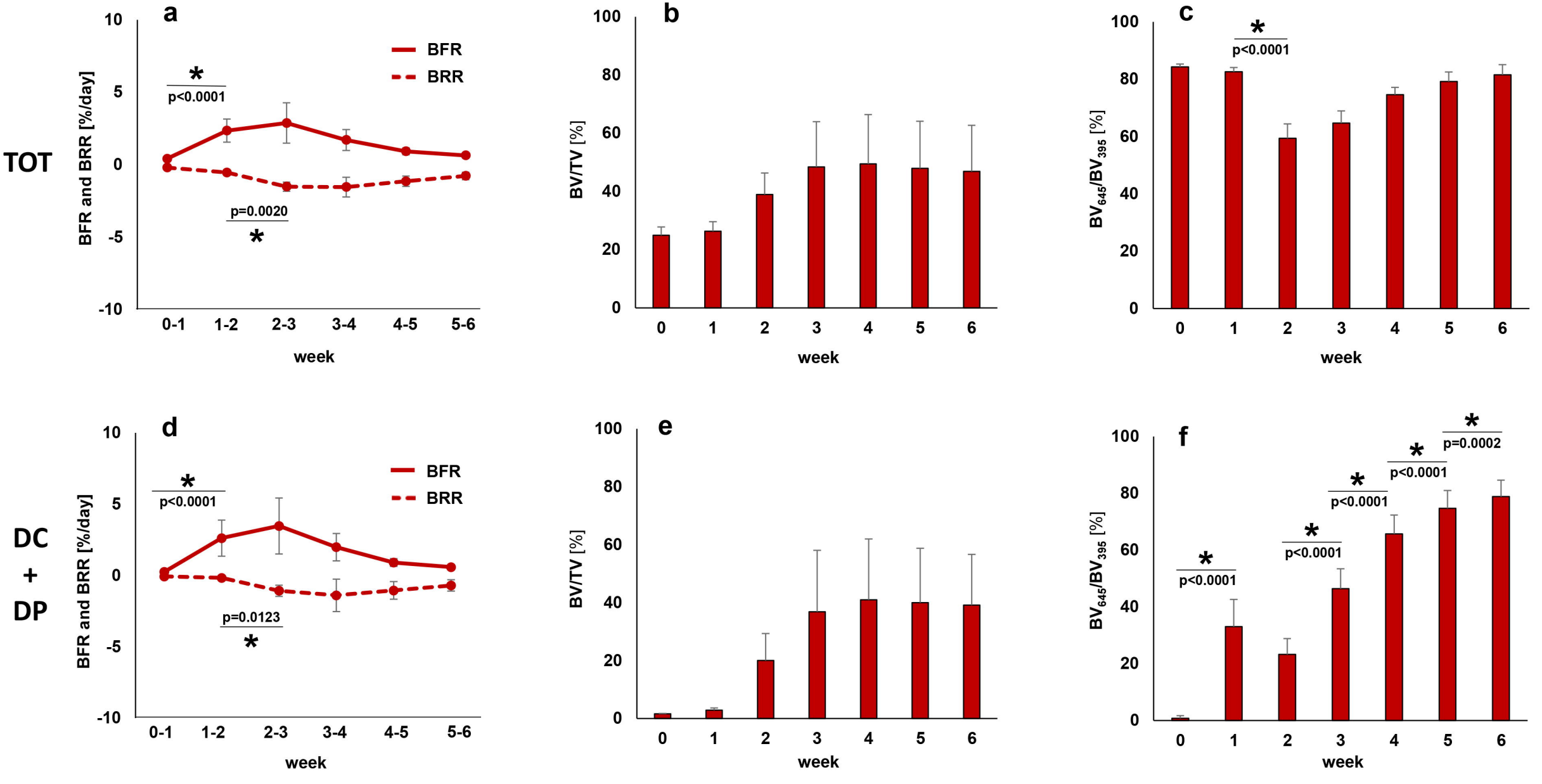
TOT
DC + DP
a
b
c
d
e
f
BFR
BRR
BFR and BRR [%/day]
BV/TV [%]
$BV_{645}/BV_{395}$ [%]
week
0-1
1-2
2-3
3-4
4-5
5-6
p<0.0001
p=0.0020
p=0.0123
p=0.0002

Figure 4

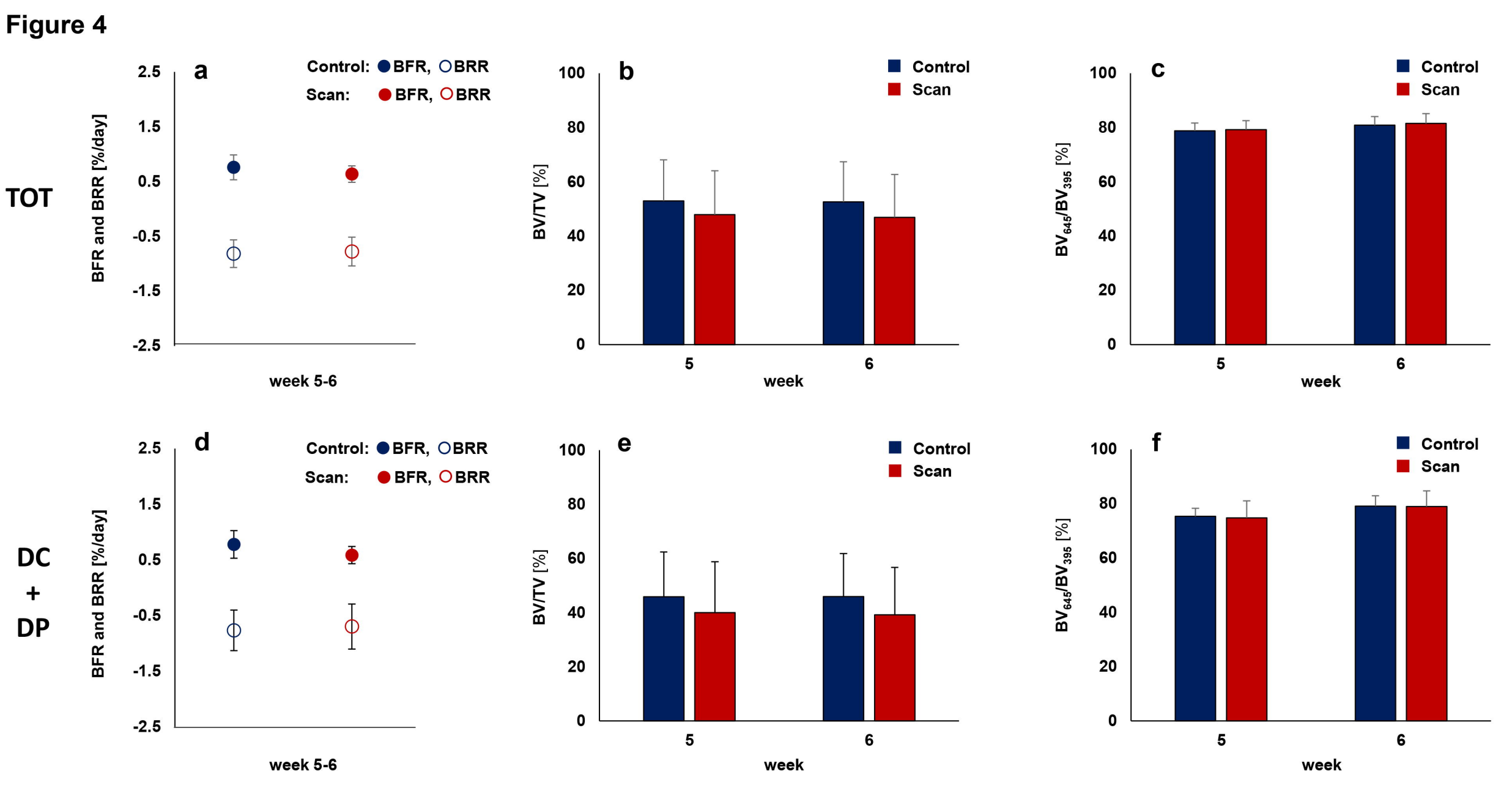
TOT
DC + DP
a
b
c
d
e
f
Control: BFR, BRR
Scan: BFR, BRR
BFR and BRR [%/day]
2.5
1.5
0.5
-0.5
-1.5
-2.5
week 5-6
BV/TV [%]
100
80
60
40
20
0
Control
Scan
5
6
week
BV645/BV395 [%]

Figure 5